Hossein Ghiassian · Soheil Ghareh

Stability of sandy slopes under seepage conditions

Abstract Stability against shallow mass sliding in saturated sandy slopes under seepage depends on the flow direction and hydraulic gradient, particularly near the ground surface. Two modes of instability i.e., Coulomb sliding and liquefaction have been studied and the critical flow directions discussed. The utility of the numerical approach in solving complex flow problems with irregular boundaries and surface topography is demonstrated by means of two slope examples with different internal drainage conditions. The numerical results for the seepage gradients at different points are compared with those predicted by the simple expression derived in this study, and the corresponding effects on the stability are evaluated.

Keywords Landslide · Infinite slope · Seepage · Horizontal drain · Flownet

Introduction

Sandy slopes may be dry, moist, or saturated as a result of surface flow, infiltration or seepage. Saturated slopes with seepage are the most critical. In this situation, the slope may fail as a result of greatly reduced shear resistance and shear failure along a critical sliding surface. Alternatively, the slope may fail as a result of complete loss of effective contact stress between particles and subsequent liquefaction.

Many references in the literature describe the slope failure or landslide due to seeping water, and define the process by different terms as piping, sapping or spring sapping, internal erosion, subsurface or seepage erosion, and tunnel scouring (Terzaghi and Peck 1967; Hutchinson 1968, 1982; Higgins 1984; Iverson and Major 1986; Jones 1990; Dunne 1990; Hagerty 1991a, b; Koenders and Selimeyer 1992; Worman 1993; Skempton and Brogan 1994). Distinctions have however been made by some investigators between different mechanisms involved in the instability caused by seepage (Dunne 1990; Crosta and Prisco 1999).

Iverson and Major considered the possibility of both liquefaction and Coulomb sliding for hillslope failure and debris flow mobilization. For some upward seepage conditions, slope stability is limited by static liquefaction rather than by Coulomb failure. Close association between these liquefaction conditions and certain Coulomb failure conditions tends to initiate spontaneous and catastrophic flowage of the soil mass. This study however considers the seepage gradient as an independent component with respect to the flow regime. A condition that may occur for cases such as an artesian seepage condition where the gradient is mainly controlled by the artesian system rather than the slope itself whereas in normal situations where the slope becomes saturated due to the rainfall and subsequent runup, the slope configuration in fact influences the seepage pattern in regard to both seepage direction and gradient. The study presented here attempts to elaborate this subject by presenting the results of some seepage analysis and corresponding effects on the slope stability. The stability is considered only in view of soil mass movement (landsliding), not surficial erosion, although sandy slopes are susceptible to both types of failure. The former instability typically occurs on slopes steeper that 2:1 (horizontal to vertical) during periods of prolonged or intense rain or due to excessive irrigation or waterline breaks. Surficial erosion, on the other hand, is due to the wearing away of soil particles by tractive stresses exerted via overland flow, wind, and ice.

Coulomb sliding failure

A saturated slope under seepage condition is shown in Fig. 1. The magnitude of the seepage force F_w is directly proportional to the hydraulic gradient 'i' and the soil volume. The gradient can be derived as a function of seepage direction (λ) and slope angle (β), as depicted in the figure. This is in fact an "*exit*" gradient for a locally uniform seepage.

$$i = \frac{\sin \beta}{\sin \lambda} \tag{1}$$

Some important seepage directions and corresponding values of hydraulic gradient are presented in Table 1.

Infinite slope theory

The so-called infinite slope model can be used to analyze translational slope movement. The failed mass progresses along a more or less planar surface approximately parallel to the ground surface, with little rotary movement or backward tilting characteristic of rotational slides or slumps (Schuster and Krizek 1978). The movement of translational slides is normally controlled by surfaces of weakness, such as faults, joints, bedding planes, and variations in shear strength between layers of bedded deposits. A translational slide can also occur in homogeneous slopes of coarse-textured, cohesionless soil such as sand dunes, sandy banks, and levees. In the infinite slope analysis of homogeneous slopes, the slip surface is assumed to be a plane parallel to the ground surface where the end effects can be neglected (Huang 1982). This analysis is valid if the ratio of depth to length of the sliding mass is small (a ratio of 1/20 or less is commonly used).

An infinite slope element subjected to both uniform seepage and gravitational forces is shown in Fig. 2. For the sake of convenience and efficiency, the "*seepage force*" approach is used although the "*boundary pore pressure*" approach gives identical results (Lambe and Whitman 1969). In the former approach, only the buoyant weight of an element and the seepage force are considered in the equilibrium equations; boundary water forces are not required.
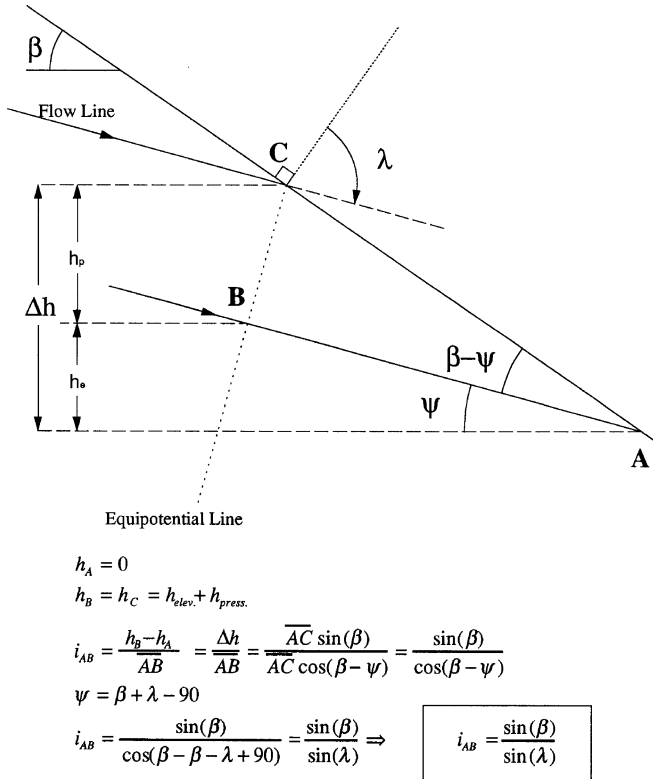
$h_A = 0$

$h_B = h_C = h_{elev.} + h_{press.}$

$i_{AB} = \dfrac{h_B - h_A}{AB} = \dfrac{\Delta h}{AB} = \dfrac{\overline{AC}\sin(\beta)}{\overline{AC}\cos(\beta - \psi)} = \dfrac{\sin(\beta)}{\cos(\beta - \psi)}$

$\psi = \beta + \lambda - 90$

$i_{AB} = \dfrac{\sin(\beta)}{\cos(\beta - \beta - \lambda + 90)} = \dfrac{\sin(\beta)}{\sin(\lambda)} \Rightarrow \boxed{i_{AB} = \dfrac{\sin(\beta)}{\sin(\lambda)}}$

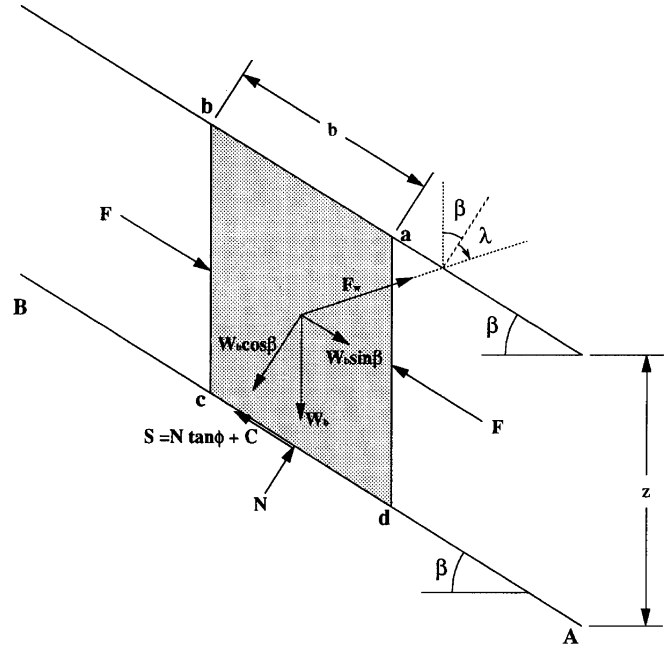**Fig. 1** Derivation of exit seepage gradient in slopes with locally uniform flow

Fig. 2 Forces acting in an infinite slope subjected to gravitational body or soil weight force (W_b), and seepage force (F_w) with a variable seepage direction $0 < \lambda < (180° - \beta)$

$$F.S. = \dfrac{\cos\beta - i\frac{\gamma_w}{\gamma_b}\cos\lambda}{\sin\beta + i\frac{\gamma_w}{\gamma_b}\sin\lambda}\tan\phi' + \dfrac{\frac{c'b}{W_b}}{\sin\beta + i\frac{\gamma_w}{\gamma_b}\sin\lambda}$$

The safety factor expression of the element in Fig. 2 can be derived as follows:

$$F.S. = \dfrac{\cos\beta - A_b\cos\lambda}{\sin\beta + A_b\sin\lambda}\tan\phi' + \dfrac{m_b}{\sin\beta + A_b\sin\lambda} \tag{2}$$

$W_b = V\gamma_b = zb\cos\beta\gamma_b$

where:

$F_w = iV\gamma_w$

$A_b = i\dfrac{\gamma_w}{\gamma_b} = \dfrac{\sin\beta}{\sin\lambda}\dfrac{\gamma_w}{\gamma_b}$

$N = W_b\cos\beta - F_w\cos\lambda$

$m_b = \dfrac{cb}{W_b} = \dfrac{c}{\gamma_b z\cos\beta}$

$S = N\tan\phi' + c'b = (W_b\cos\beta - F_w\cos\lambda)\tan\phi' + c'b$

A_b and m_b are called the buoyant seepage and buoyant cohesion coefficients respectively.

For cases in which $c' = 0$, the factor of safety simplifies to:

$F.S. = \dfrac{S}{W_b\sin\beta + F_w\sin\lambda} = \dfrac{(W_b\cos\beta - F_w\cos\lambda)\tan\phi' + c'b}{W_b\sin\beta + F_w\sin\lambda}$

$$F.S. = \dfrac{\cos\beta - A_b\cos\lambda}{\sin\beta + A_b\sin\lambda}\tan\phi \tag{3}$$

Table 1 Common flow directions and corresponding hydraulic gradients

Limiting cases	Seepage direction	Hydraulic gradient
Parallel flow	$\lambda = 90°$	$i = \sin\beta$
Horizontal flow	$\lambda = 90° - \beta$	$i = \tan\beta$
Nearly normal (upward) flow	$\lambda \to 0$	$i \to \infty$
Vertical (downward) flow	$\lambda = 180° - \beta$	$i = 1$

For F.S.=1 and assuming $\gamma_{sat} \approx 2\gamma_w$, Eq. (4) establishes the relationship between critical slope angle (β_{crit}) for a given seepage vector (i and λ) and friction angle ϕ'.

$$\tan \phi' \approx \frac{\sin \beta_{crit} + i \sin \lambda}{\cos \beta_{crit} - i \cos \lambda} \qquad (4)$$

Limiting cases

Case (1)
  Parallel flow ($\lambda=90°$, $i=\sin \beta$)

$$\tan \phi' \approx \frac{\sin \beta_{crit} + \sin \beta_{crit} \sin 90°}{\cos \beta_{crit} - \sin \beta_{crit} \cos 90°} \approx 2\frac{\sin \beta_{crit}}{\cos \beta_{crit}}$$

$$\approx 2\tan \beta_{crit} \Rightarrow \beta_{crit} \approx \tan^{-1}(0.5 \tan \phi')$$

Case (2)
  Vertical (downward) flow ($\lambda=180°-\beta$, $i=1$)

$$\tan \phi' \approx \frac{\sin \beta_{crit} + \sin(180° - \beta_{crit})}{\cos \beta_{crit} - \cos(180° - \beta_{crit})}$$

$$\approx \frac{2\sin \beta_{crit}}{2\cos \beta_{crit}} \approx \tan \beta_{crit} \Rightarrow \beta_{crit} \approx \phi'$$

Case (3)
  Horizontal Flow ($\lambda=90°-\beta$, $i=\tan \beta$)

$$\tan \phi' \approx \frac{\sin \beta_{crit} + \tan \beta_{crit} \sin(90° - \beta_{crit})}{\cos \beta_{crit} - \tan \beta_{crit} \cos(90° - \beta_{crit})}$$

$$\approx \frac{\sin \beta_{crit} + \tan \beta_{crit} \cos \beta_{crit}}{\cos \beta_{crit} - \tan \beta_{crit} \sin \beta_{crit}} \approx \frac{\tan \beta_{crit} + \tan \beta_{crit}}{1 - \tan^2 \beta_{crit}}$$

$$\approx \frac{2\sin \beta_{crit} \cos \beta_{crit}}{\cos^2 \beta_{crit} - \sin^2 \beta_{crit}} \approx \tan 2\beta_{crit}$$

$$\beta_{crit} \approx 0.5\phi'$$

A summary of the above derivations is presented in Table 2. The minimum stability against Coulomb sliding in the above three cases occurs when seepage direction is $\lambda=90°-\beta$ which corresponds to a horizontal flow. The stability can decrease even more if seepage emerges from the slope with a smaller λ. The most critical seepage gradient is when the flow direction approaches zero, i.e., perpendicular to the slope ($i \rightarrow \infty$).

Liquefaction failure
A static, saturated cohesionless mass of soil will liquefy when subjected to a seepage force that has an upward, vertical component equal in magnitude to the submerged weight of the soil. In this case, effective contact stresses between all particles go to zero and the soil loses all its strength and deforms by "*flowing*"

rather than by "*frictional*" sliding. The condition for liquefaction in terms of the variables (λ, β) and geometry of Fig. 2 can be expressed by (Iverson and Major 1986):

$$A_b \cos[(\lambda + \phi') + (\beta - \phi')] = 1 \qquad (5)$$

For a condition of $\lambda=-\beta$, i.e., vertically upward seepage, this equation is satisfied if $A_b=1$. However, this state or condition may be impossible to attain. The analysis presented by Iverson and Major is based on an assumption that the components of seepage vector viz., gradient i and direction λ, vary independently. While this assumption may be justified for cases of non-uniform flow such as an artesian seepage condition where the gradient is mainly controlled by the artesian system rather than the slope itself, it is not applicable to the seepage condition in Fig. 1 where the gradient (i) is a function of λ (Eq. 1). Using this equation and setting $\lambda=-\beta$, the magnitude of A_b becomes -1 which is different from the value predicted by Eq. (5). This contradiction arises because the condition of $\lambda=-\beta$ is beyond the acceptable range of λ which is from zero to $180°-\beta$.

Failure mode criteria
By substituting Eq. (1) into Eqs. (3) (F.S.=1) and (5), and assuming $\gamma_b=\gamma_w$, the limiting seepage direction λ_{crit} for generating Coulomb sliding or liquefaction failure can be obtained for various values of slope angle β and friction angle ϕ'.

$$\lambda_{crit} \leq \tan^{-1}\left(\frac{\tan \beta \tan \phi'}{\tan \phi' - 2\tan \beta}\right) \qquad \text{(Coulomb sliding)} \qquad (6)$$

$$\lambda_{crit} \leq \tan^{-1}\left(\frac{\tan \beta}{2\tan^2 \beta + 1}\right) \qquad \text{(liquefaction)} \qquad (7)$$

These results have been plotted in Fig. 3 for various seepage direction (λ), slope angle (β), and effective friction angle (ϕ'). It can be seen in this figure that Coulomb failure always preempts or coincides with liquefaction failure. This result is slightly different from the findings presented by Iverson and Major in which liquefaction failure may preempt Coulomb failure under some circumstances.

The influence of seepage direction on the stability of infinite slopes can also be shown in terms of its effect on the factor of safety as shown in Fig. 4. The ratio of safety factor for cohesionless slopes with seepage to that for dry slopes has been plotted versus seepage direction for various slope angles. The stability of a previously dry slope drops by one-half (assuming $\gamma_b=\gamma_w$) when water seeps parallel to the slope ($\lambda=90°$). The stability is decreased even more when the seepage emerges from the slope ($\lambda<90°$). On the other hand, the stability is equivalent to that of a dry slope when the water flows vertically downward ($\lambda=180°-\beta$).

Table 2 Critical slope angles for various seepage directions

Seepage direction	λ	i	β_{crit}	β_{crit} (for $\phi'=30°$)
Vertical	$180°-\beta$	1	ϕ'	30°
Parallel	90°	$\sin \beta$	$\tan^{-1}(0.5 \tan \phi')$	16.1°
Horizontal	$90°-\beta$	$\tan \beta$	$0.5\phi'$	15°

Fig. 3 Analysis of slopes for liquefaction and Coulomb sliding failure
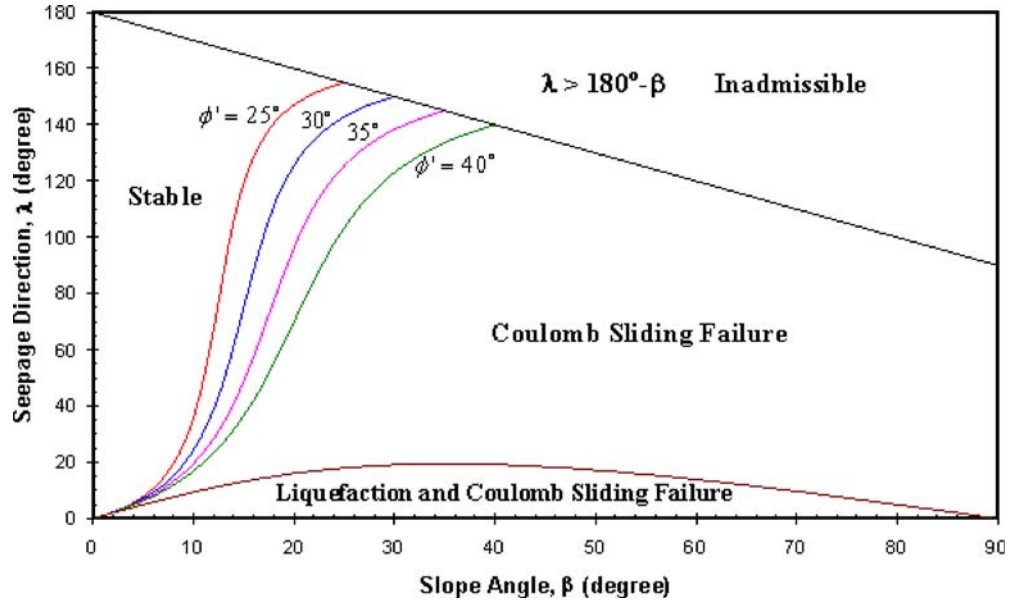
Seepage analysis

The stability analysis presented in Fig. 2 for an infinite slope with water flow assumed that the seepage condition was identical at all points vertically downward the slope, i.e., locally uniform. In reality, however, boundary conditions can influence the flow regime in the slope, particularly in the vicinity of the boundaries. This effect would be more pronounced if drains exist in the slope. In the following sections, two slope configurations are considered, and flow nets have been obtained using a numerical approach. Then, the actual seepage gradient and the flow direction at all points in the slope are compared to those assumed in the analysis (Fig. 1). Finally, the implementations of these differences on the stability are discussed.

Numerical solution

A numerical approach based on the Laplace equation was employed to obtain the flow net in the slope. The Laplace equation for three-dimensional flow in porous media is expressed as:

$$\frac{\partial^2 h}{\partial x^2} + \frac{\partial^2 h}{\partial y^2} + \frac{\partial^2 h}{\partial z^2} = 0 \tag{8}$$

where h=hydraulic or piezometric head at any point, equal to the sum of h_e (the elevation head) and h_p (the pressure head). The solution of the above equation for any given set of boundary conditions is a function $h(x, y, z)$ that describes the value of head at any point in the field. This solution can be used to produce a

Fig. 4 Influence of seepage on the stability of sandy slopes as a function of slope angle (β) and seepage direction (λ)
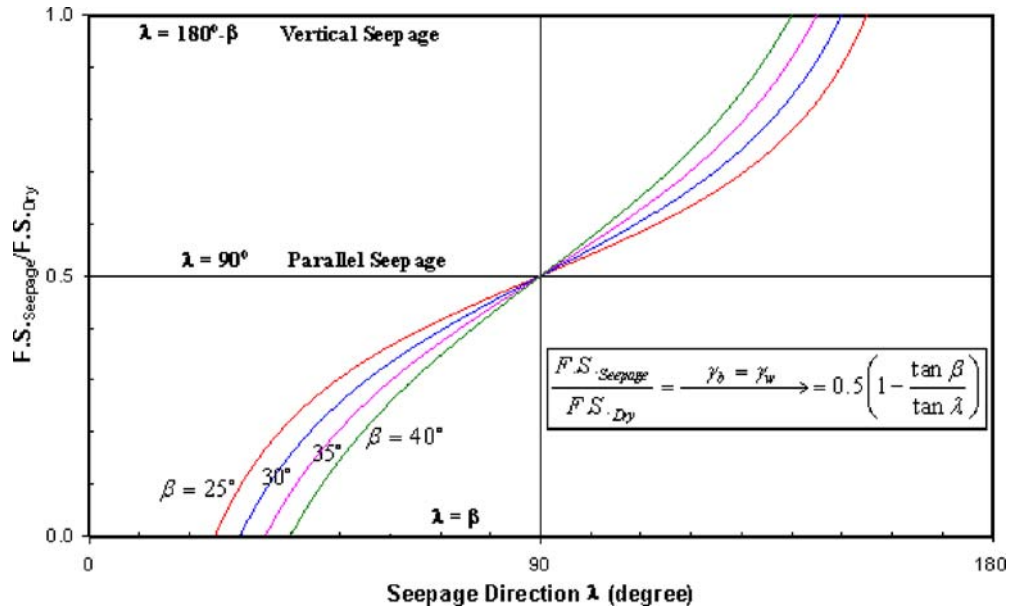
contoured equipotential map of h and/or a flow net. For a two-dimensional flow field, the solution becomes a function $h(x, y)$.

The fundamental analytical technique for solving boundary-value problems such as the Laplace equation is separation of variables (Pipes 1958; Pinsky 1991). However, this technique does not work on all equations. It is not clear which equation can or can not be solved by this method. Powers (1972) states that the region in which the solution is to be found also limits the applicability of the method. He states that the region must be a "generalized rectangle" which means a region described by inequalities whose endpoints are fixed. Freeze and Cherry (1979) state that there is no exact analytical solution for a trapezoidal region except in the case of impermeable top and bottom end boundaries. An approximate solution for this case was presented by Toth (1962); however, it appears to be satisfactory only for small ground slopes of about 3° or less (Toth 1963).

Numerical methods can solve many complex flow problems for irregular regions, boundary conditions, and geohydrologic settings. These methods often use the finite-difference technique applied to the Laplace equation. This iterative technique is based on a "relaxation process" that simultaneously calculates hydraulic heads at various node points in a network (Shaw and Southwell 1941; Freeze and Witherspoon 1966, 1967). The iteration continues until the difference between two consecutively computed heads at all points become very small. The technique is simple and efficient for solving a set of finite-difference equations. Numerical methods are also capable of treating general, nonhomogeneous, anisotropic, and three-dimensional problems (Southwell 1946; Freeze and Witherspoon 1966, 1967). Electronic spreadsheets have also been used successfully to solve finite-difference problems by the relaxation technique (Das 1983; Kleiner 1985). Many finite-difference problems, which previously required fairly sophisticated programming, can be solved with relative ease and adequate accuracy on a spreadsheet. The solutions presented here are based on the spreadsheet solution. Calculated values of the hydraulic heads or stream potentials at nodal points were used to plot contours of equipotential lines or flow lines.

Slopes with no drain

A generic configuration of a slope with a flat surface and two horizontal and vertical impervious boundaries is shown in Fig. 5. It is assumed that the slope is at $\beta = 45°$, under a fully saturated condition, and a steady seepage is established. While a full saturation condition may not always exist in field situations, the treatment of the slope surface here as a piezometric surface is reasonable. According to Toth (1962) and Freeze and Witherspoon (1966), there is, in general, a close correlation of the piezometric surface with the slope topography, and the average water table position for an unconfined flow system can be viewed as a subdued replica of the surface topography. Besides, the assumed full saturation represents the most critical situation that the slope may experience with respect to the mass stability.

It can be realized in Fig. 5 that the flow direction is not generally uniform at any point. Exceptions exist for specific boundary conditions which may rarely occur in the field (Ghiassian 1996). It is seen that at the upper face of the slope, water is seeping into the slope (recharge) whereas at the lower face, water is emerging from the slope (discharge). The most critical part of the slope with respect to the mass stability and piping resistance would be near the toe where emerging seepage occurs and the seepage angle is the
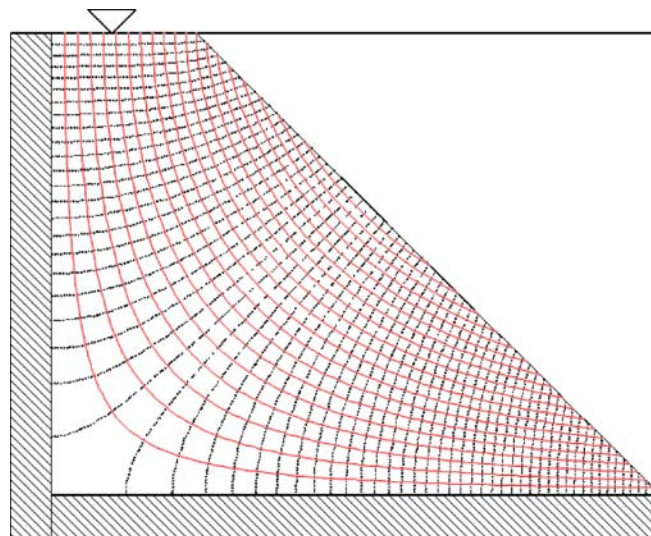

Fig. 5 Flow lines (*contours*) obtained by a numerical analysis for slope with vertical and horizontal impervious boundaries, and no drain

smallest. Conversely, the top of the slope is more stable since the seeping water in this region will increase the component of effective stress normal to a potential failure surface. The maximum seepage angle occurs right at the crest of the slope, where seepage is vertically downward.

It should be noted that Eq. (1) was derived based on an assumption that the seepage direction near the slope surface (exit region) was locally uniform. In order to evaluate the accuracy of Eq. (1) in calculating the gradients at deep points in the slope, a comparison can be made between the gradients calculated from Eq. (1) and the actual gradients calculated from the numerical solution (see Fig. 6), by defining gradient ratio (GR) as:

$$\mathrm{GR} = \frac{i_{\mathrm{uniform}}(\mathrm{From\ Fig.1})}{i_{\mathrm{real}}(\mathrm{From\ Fig.6})} \qquad (9)$$

Figure 7 illustrates the variation of GR in the slope. It is seen that the value of GR increases with depth. Near the slope face, GR becomes almost one, that means Eq. (1) gives an accurate estimation of the gradient. This zone in the slope, in fact, appears to be where an infinite slope failure is likely to occur. At deeper points in the slope, where boundary condition effects gradually become important to influence the flow regime, and consequently the stability, GR becomes larger than one, meaning that the gradient calculated by Eq. (1) is deviating from the real value; therefore it is not accurate. Nevertheless as mentioned above, the Coulomb sliding failure would occur at shallow depths, indicating that the use of simple expression 1 for the gradient evaluation should be sound and justified. If the critical seepage direction is uniform over a large portion of the slope surface, the translational instability would expect to occur in this portion, with an associated higher slide thickness. A real example for this condition is often seen in the lower portions of natural slopes where a fairly uniform seepage parallel to the slope face ($\lambda = 90°$) is reached (Lambe and Whitman 1969).

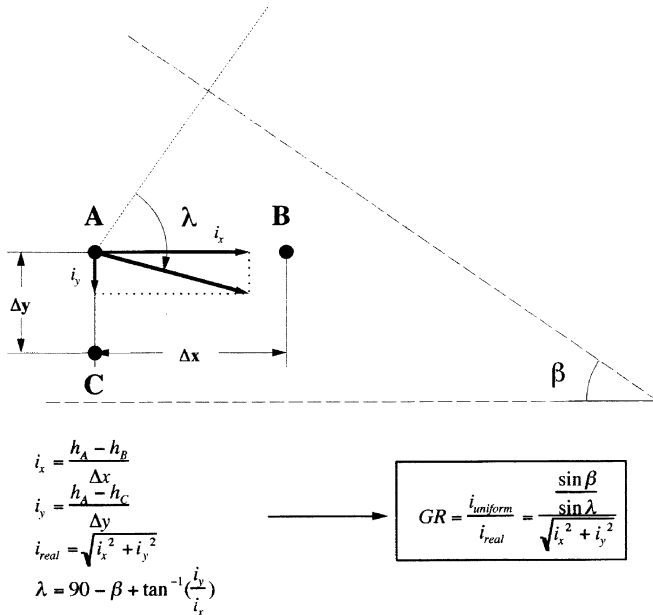$$i_x = \frac{h_A - h_B}{\Delta x}$$

$$i_y = \frac{h_A - h_C}{\Delta y}$$

$$i_{real} = \sqrt{i_x^2 + i_y^2}$$

$$\lambda = 90 - \beta + \tan^{-1}\left(\frac{i_y}{i_x}\right)$$

$$GR = \frac{i_{uniform}}{i_{real}} = \frac{\dfrac{\sin\beta}{\sin\lambda}}{\sqrt{i_x^2 + i_y^2}}$$

Fig. 6 Determination of gradient ratio (GR) from the total heads at nodal points in finite-difference numerical solution of flownet

Slopes with drain

The preceding example shows that the boundary conditions can influence the flow field significantly. The flow field, in turn, can greatly affect the stability of a sandy slope as explained before. It was shown in Fig. 3 that the mass stability decreases as the seepage direction (λ) becomes smaller and flow starts emerging from the

slope. The resistance to piping is also dependent on the seepage angle at the exit points. At small seepage angles, seepage forces exceed intergranular stresses or forces of cohesion, and cause the detachment and movement of soil particles. Once a pipe forms, it enlarges quickly because of further concentration of flow lines in the pipe area. Therefore, the most vulnerable portion of a slope for surficial instability is where water is emerging from the slope, i.e., the discharge area. In these situations, where groundwater appears to be a major detrimental factor on the stability, horizontal drains have proved to be a cost-effective and viable measure in preventing and correcting the failure (Smith and Stafford 1955; Tong and Maher 1975; Kenney et al. 1977; Barrett 1980; Ruff 1980; Nonveiller 1981; Chan 1987; Singer 1990; Whiteside 1997; Cai et al. 1998; Rahardjo et al. 2003). They act effectively only when the ground is sufficiently permeable to allow drainage.

Figure 8 shows the influence of a horizontal drain on the flow field in the slope example. It is seen that the horizontal drain causes the flow direction in the slope changes favorably in regard to the mass stability, with this effect more pronounced in the vicinity of the drain. Some portion of the collected water comes to the surface through the drain where it once again becomes beneficial recharge. This is clear in Fig. 8 by comparing the number of stream channels entering the drain to the number of channels exiting the drain. Since all channels transmit an equal amount of water per unit time (flow rate), it is quite obvious that some portion of the water in the drain should come to the surface to flow over the slope face as runup.

The variation of GR, similar to the case of the slope with no drain, was examined as shown in Fig. 9. It is clear that some portion of the slope above the drain is greatly affected by the drain such that the GR values at points near the drain are even less than

Fig. 7 Variation of gradient ratio (GR) for slope with vertical and horizontal impervious boundaries, and no drain
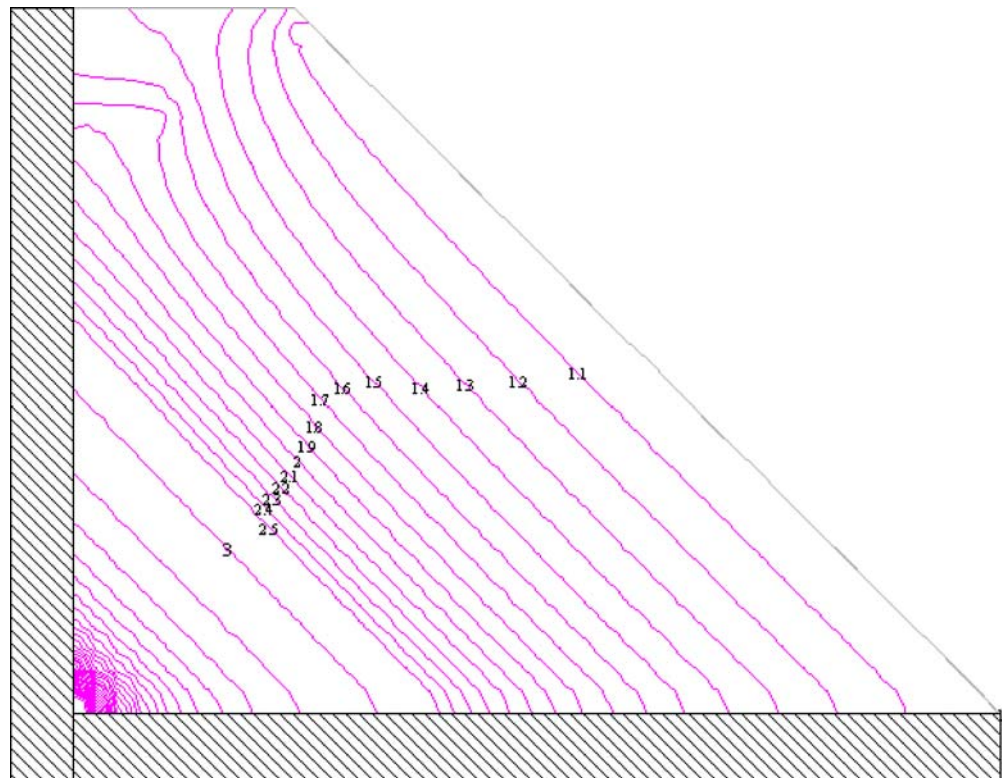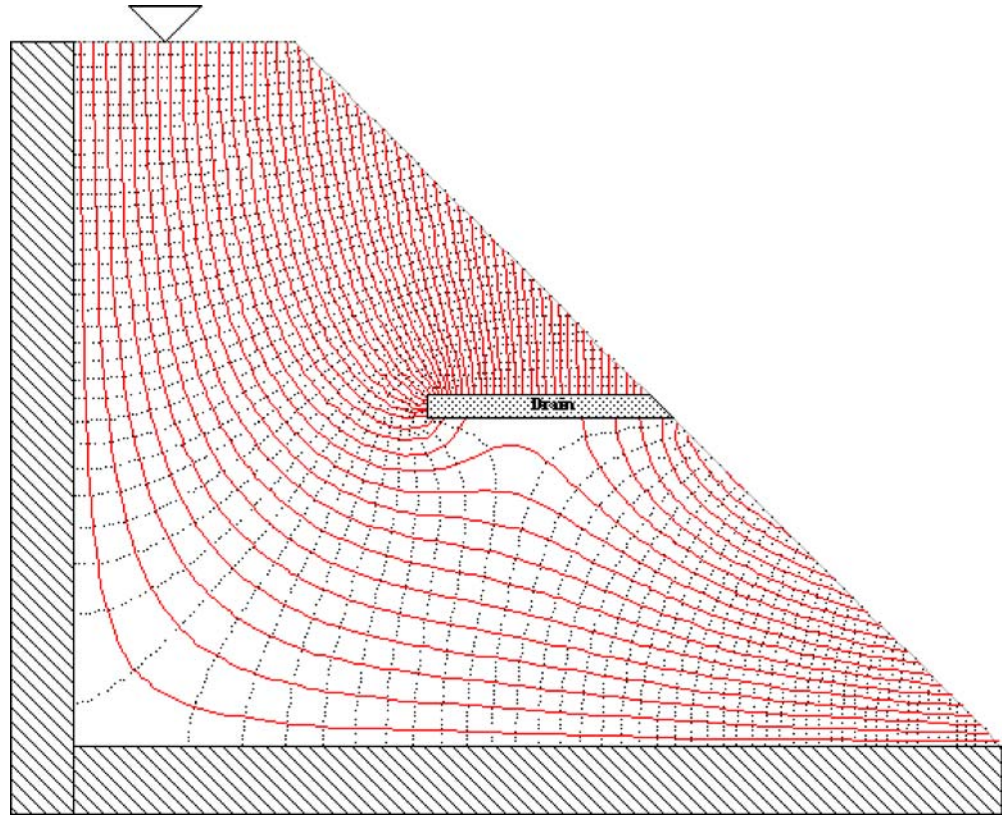
Fig. 8 Flow lines (*contours*) obtained by a numerical analysis for slope with vertical and horizontal impervious boundaries and horizontal drain

one. This means that the gradient calculated by Eq. (1) is smaller than the real values obtained from the flow net. Therefore, the stability analysis based on Eqs. (1) and (3) for the portion of the slope above the drain would be less conservative. On the other hand, the lower portion of the slope below the drain is influenced such that the trend of the GR change is similar to that observed for the slope with no drain (Fig. 7) although the variation of GR is much more abrupt, particularly in the vicinity of the drain.

Fig. 9 Variation of gradient ratio (GR) for slope with vertical and horizontal impervious boundaries, and horizontal drain
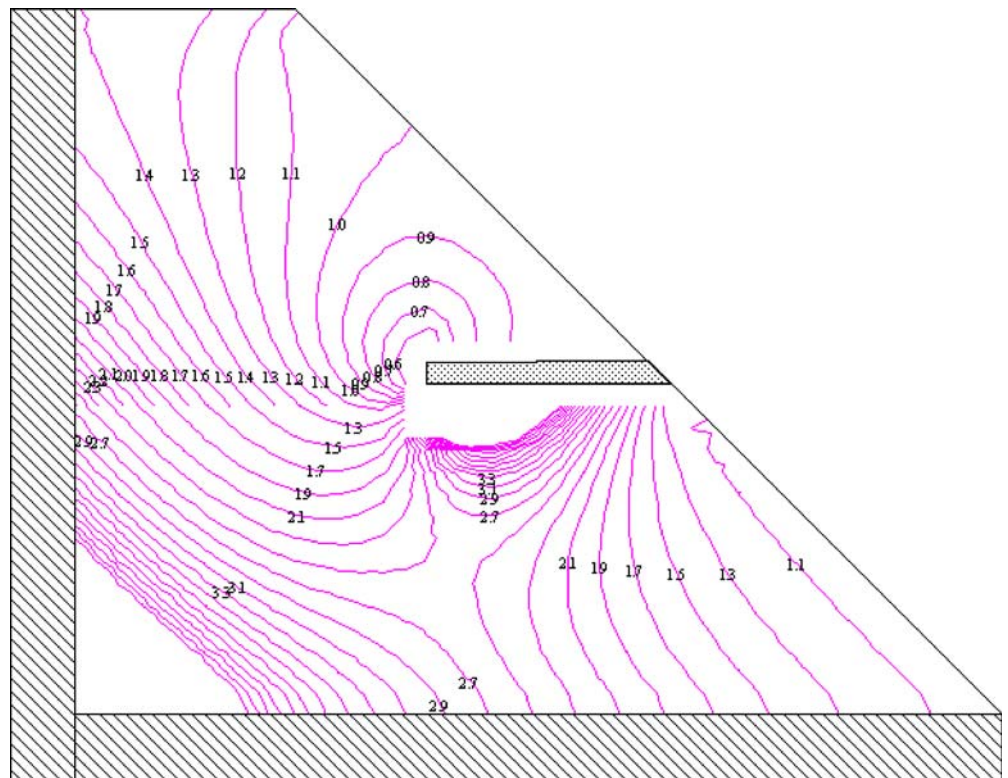
Therefore, the stability analysis based on Eq. (1) for the slope portion below the drain would still be conservative.

It was realized that the presence of a horizontal drain in the slope can cause the flow direction to become vertically downward, which in turn can increase the stability of the slope significantly. In order to better understand this important effect, the variation of local safety factor ratios, defined as F.S.seepage/F.S.dry, are shown in Figs. 10 and 11 for the plain slope and the slope with the drain, respectively. The safety factors have been calculated using the local hydraulic gradient (i) and seepage direction (λ) values at specific (nodal) points within the slope according to the following expressions.

$$\left\{\begin{array}{c} \text{F.S.}_{\text{seepage}} = \frac{\cos\beta - A_b\cos\lambda}{\sin\beta + A_b\sin\lambda}\tan\phi \\ \text{F.S.}_{\text{dry}} = \frac{\tan\phi}{\tan\beta} \end{array}\right\}$$
$$\Rightarrow \frac{\text{F.S.}_{\text{seepage}}}{\text{F.S.}_{\text{dry}}} = \frac{\sin\beta - A_b\cos\lambda\tan\beta}{\sin\beta + A_b\sin\lambda} \tag{10}$$

The great influence of the horizontal drain in increasing the stability of the slope particularly at shallow depths near the slope face can be realized from the comparison between these two figures. This effect, however, gradually diminishes by moving away from the drain. It is seen in Fig. 10 that the stability increases by moving toward the upslope due to the increase of the seepage direction. This effect of the seepage orientation is more evident in Fig. 11 where the stability around the drain has increased remarkably due to the vertical downward seepage direction caused by the drain. The portion of the slope above the drain appears to benefit further from the stabilizing influence of the drain compare to the lower portion below the drain. However, in actual situations, this effect is mainly controlled by the vertical spacing and

dimension of the drains (Cai et al. 1998). Also, it can be concluded from Fig. 11 that for cases of one drainage layer, horizontal drains are most effective when located at the base of a slope, as also reported previously by Rahardjo et al. (2003).

Conclusions

The mass stability of homogenous, saturated sandy slopes under seepage were considered in view of both Coulomb sliding and liquefaction failures. Numerical seepage analyses were performed for the two slope examples with and without horizontal drains, and the hydraulic gradient results were compared with those determined by Eq. (1). Important conclusions from this study can be summarized as follows:

– The most critical stability condition is when the flow direction approaches zero ($\lambda = 0°$), i.e., perpendicular and emerging from the slope, and the least critical condition is when the flow direction is vertically downward ($\lambda = 180° - \beta$).
– Coulomb sliding failure always preempts or coincides with liquefaction failure.
– In slopes with no drain, the exit seepage gradient can be obtained by the simple expression given in Eq. (1), which gives a conservative estimate of the gradient at any point in the slope. This predicted value approaches the exact as the depth of the point from the slope surface decreases.
– In slopes with horizontal drains positioned at the slope face, the estimation of the gradient by Eq. (1) for the slope portion above the drain would result in a less conservative stability analysis. Conversely, for the slope portion beneath the drain, the results are similar to those for the slope without drain but with the effect more pronounced.

Fig. 10 Variation of local factor of safety ratio (F.S.seepage/F.S.dry) for slope with vertical and horizontal impervious boundaries, and no drain
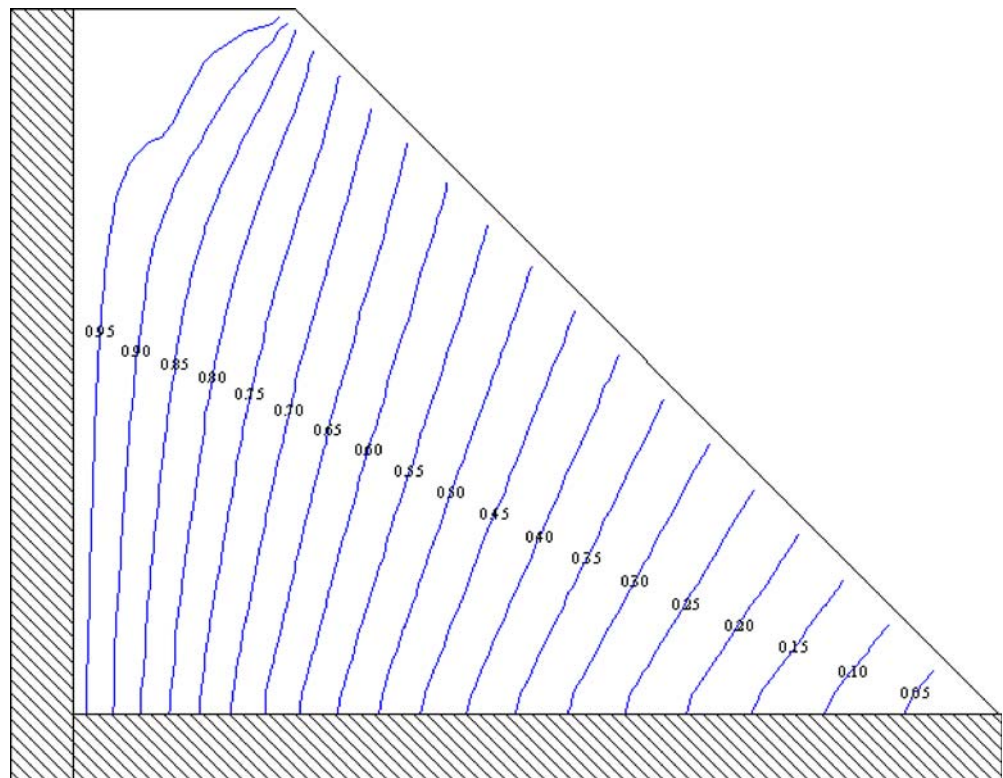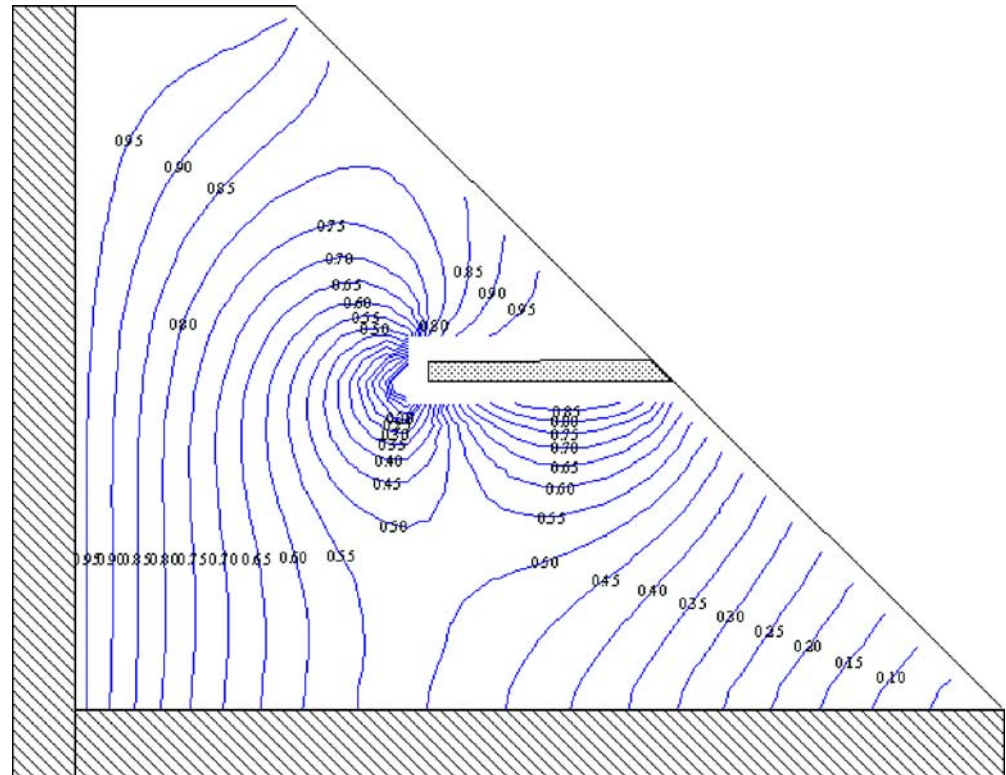
Fig. 11 Variation of local factor of safety ratio (F.S._seepage/F.S._dry) for slope with vertical and horizontal impervious boundaries, and horizontal drain

– The influence of a horizontal drain in increasing the mass stability was demonstrated by counters of safety factor ratios; this effect appears to be significant particularly for the areas around the drain.

References

Barrett RK (1980) Use of horizontal drains: case history from the Colorado division of highways. Transp Res Rec 783:20–25

Cai F, Ugai K, Wakai A, Li Q (1998) Effects of horizontal drains on slope stability under rainfall by three-dimensional finite element analysis. Comput Geotech 23(4):255–275

Chan RKS (1987) Use of horizontal drains to stabilize a steep hillside in Hong Kong. Proceedings of the 9th European Conference of Soil Mechanics & Foundation Engineering, Dublin

Crosta G, Prisco C (1999) On slope instability induced by seepage erosion. Canadian Geotechnical Journal 36:1056–1073

Das BM (1983) Advanced soil mechanics. McGraw-Hill, New York, N.Y

Dunne T (1990) Hydrology, mechanics, and geomorphic implications of erosion by subsurface flow. Geol Soc Amer, Spec Pap 252:1–28

Freeze RA, Cherry JA (1979) Groundwater. Prentice-Hall, New Jersey

Freeze RA, Witherspoon PA (1966) Theoretical analysis of regional groundwater flow: 1. Analytical and numerical solutions to the mathematical model. Water Resour Res 2:641–656

Freeze RA, Witherspoon PA (1967) Theoretical analysis of regional groundwater flow: 2. Effect of water-table configuration and subsurface permeability variation. Water Resour Res 3:623–634

Ghiassian H (1996) Stabilization of sandy slopes with anchored geosynthetic systems. Thesis submitted in partial fulfillment for the degree of Doctor of Philosophy, The University of Michigan, Ann Arbor, MI

Hagerty DJ (1991a) Piping/sapping erosion. I: basic considerations. J Hydraul Eng 17:991–1008

Hagerty DJ (1991b) Piping/sapping erosion. II: identification—diagnosis. J Hydraul Eng 17:1009–1025

Higgins CG (1984) Piping and sapping; development of landforms by groundwater outflow. Allen & Unwin, Boston, pp 18–58

Huang R (1982) Slope stability analysis. Van Nostrand Reinhold, New York

Hutchinson JN (1968) Field meeting on the coastal landslides of Kent. Proc Geol Assoc 79(Part II):227–237

Hutchinson JN (1982) Damage to slopes produced by seepage erosion in sands. In: Landslides and mudflows, Centre of International Projects, GKNT, Moscow, pp 250–265

Iverson RM, Major JJ (1986) Groundwater seepage vectors and the potential for hillslope failure and debris flow mobilization. Water Resour Res 22(11):1543–1548

Jones JAA (1990) Piping effects in humid lands. In: Groundwater geomorphology, Geol Soc Amer, Spec Pap 252, pp 111–138

Kenney TC, Pazin M, Choi WS (1977) Design of horizontal drains for soil slopes. ASCE J Geotech Eng Div 103(GT11):1311–1323

Kleiner DE (1985) Engineering with spreadsheets. Civil Eng, ASCE 55(10):55–57

Koenders MA, Selimeyer JB (1992) Mathematical model for piping. J Geotech Eng 118:943–946

Lambe TW, Whitman RV (1969) Soil mechanics. Wiley, New York

Nonveiller E (1981) Efficiency of horizontal drains on slope stability. Proc Int Conf Soil Mech Found Eng, Stockholm 3:495–500

Pinsky AM (1991) Partial differential equations and boundary-value problems with applications. McGraw-Hill, New York

Pipes LD (1958) Applied mathematics for engineers and physicists. McGraw-Hill, New York, N.Y.

Powers LD (1972) Boundary value problems. Academic, New York

Rahardjo H, Hritzuk KJ, Leong EC, Rezaur RB (2003) Effectiveness of horizontal drains for slope stability. Eng Geol 69(3–4):295–308

Ruff WT (1980) Mississippi's experience with horizontally drilled drains and conduits in soil. Transp Res Rec 783:35–38

Schuster RL, Krizek RJ (1978) Landslides. Transportation Research Board, Special Report 176, National Academy of Science, Washington D.C.

Shaw FS, Southwell RV (1941) Relaxation methods applied to engineering problems. VII, Proc. Roy. Soc. London, A178:1–17

Singer GC (1990) Use of horizontal drain holes for slope stability control. Proc 2nd International Symposium on Mine Planning and Equipment Selection, Calgary, pp 379–384

Skempton AW, Brogan JM (1994) Experiments on piping in sandy gravels. Geotechnique 44:449–460

Smith TW, Stafford GV (1955) California experience with horizontal drains for landslide correction and prevention. ASCE Annual Convention, New York City, New York October pp. 24–28

Southwell RV (1946) Relaxation methods in theoretical physics. Oxford University Press, pp 248

Terzaghi K, Peck RB (1967) Soil mechanics in engineering practice. Wiley, New York

Tong PYL, Maher RO (1975) Horizontal drains as a slope stabilizing measure. J Eng Soc Hong Kong 3(1):15–27

Toth J (1962) A theory of groundwater motion in small drainage basins in central Alberta Canada. J Geophys Res 67(11):4375–4387

Toth J (1963) A theoretical analysis of groundwater flow in small drainage basins. J Geophys Res 68(16):4795–4812

Whiteside PGD (1997) Drainage characteristics of a cut soil slope with horizontal drains. Q J Eng Geol 30:137–141

Worman A (1993) Seepage-induced mass wasting in coarse soil slopes. J Hydraul Eng 119:1155–1168

H. Ghiassian (✉) · **S. Ghareh** (✉)
College of Civil Engineering, Iran University of Science & Technology,
P.O. Box 16765-163, Narmak, Tehran 16846-13114, Iran
e-mail: h_ghiassian@iust.ac.ir
e-mail: ghareh_soheil@iust.ac.ir